ARTICLE

A rapid initial beam establishment method using material sensing in joint communications and sensing systems

Yi Geng[1]

[1] *CICT Mobile, China*

Corresponding author: Yi Geng, gengyi@cictmobile.com

Communication systems operating in high frequency bands typically utilize narrow beams to compensate significant path loss. However, achieving beam alignment between the transmitter and receiver is extremely time-consuming due to the large number of beam directions associated with narrow beams. This latency in initial beam establishment poses a significant challenge to the deployment of future 6G networks, which operate in high frequency bands. To tackle this problem, this paper proposes a novel initial beam establishment method that uses the material sensing results from joint communications and sensing systems. Specifically, by exploiting pre-identified material information of environmental reflectors, the proposed method predicts the Reflection Loss (RL) induced by each reflector. The base station prioritizes scanning directions associated with lower RL, establishing connections immediately without the need to sweep through remaining beam directions. This approach significantly reduces the latency of initial beam establishment, thereby enhancing the performance and efficiency of 6G networks.

Keywords: Beam sweeping, initial beam establishment, joint communications and sensing, material identification, reflection loss

1. INTRODUCTION

By 2030, 6G is expected to increase communication capacity by a factor of twenty compared to 5G [1]. One of the key enablers for this improvement is the use of higher frequency bands (e.g., millimeter wave (mmWave) or even terahertz (THz)), which allow for much higher bandwidths. However, operating in higher frequency bands introduces many challenges, such as significant atmospheric attenuation [2]. To compensate for the high path loss, extremely narrow beams are essential. Nonetheless, employing narrow beams significantly complicates initial beam establishment. This process aims to align a suitable beam pair, including a Base Station (BS) beam direction and a User Equipment (UE) beam direction, to ensure optimal connectivity between the BS and the UE. In 5G NR, the network exhaustively sweeps multiple Synchronization Signal Blocks (SSB) across all possible beam directions within the coverage area. UEs measure the Reference Signal Received Power (RSRP) of SSBs for each beam direction. If the RSRP in a particular direction exceeds a predefined threshold, the network establishes a connection using that beam direction. However, this procedure is considerably more challenging at higher frequencies. With narrow beams, an exhaustive beam search might require sweeping through as much as 784 directions, assuming a 3 dB beamwidth of 5° and a Field Of View (FOV) of ±70° both in azimuth and elevation, leading to significant latency in initial beam establishment.

Several studies have focused on beam alignment algorithms to reduce the latency of initial beam establishment. Hierarchical beam search algorithms employ both a wide beam codebook and a narrow beam codebook. Each wide beam direction encompasses multiple narrow beams. Initially, the BS sweeps through the wide beams to identify the most suitable wide beam. Subsequently, the algorithm focuses on sweeping the narrow

beams within that selected wide beam direction [3, 4]. Additionally, Deep Neural Network (DNN) beam alignment algorithms can predict the optimal direction by analyzing the RSRP from a subset of all available beams, thus further reducing the latency of initial beam establishment [5, 6, 7].

In the context of Joint Communications And Sensing (JCAS), sensing-assisted Beamforming (BF) can also be exploited to enhance beam alignment by utilizing sensing results [8]. Recent studies predominantly focus on scenarios where the sensing object and the communication device are co-located. Sensing results such as a vehicle's position allow the BS to direct a narrow beam precisely at the vehicle, bypassing the conventional feedback-based beam alignment method. For example, in [9], an extended Kalman filtering framework was proposed to determine the angular information of the vehicles, thereby reducing the overhead associated with communication beam tracking. In [10], a Bayesian predictive BF scheme was introduced to refine angle estimation for beam alignment. It has been verified that the sensing-assisted BF can be applied to complex roadway scenarios and improve the beam alignment accuracy [11]. Additionally, in [12], varying beamwidths have been exploited to address beam misalignment issues arising from discrepancies between the sensing target and the UE. Despite these advancements, there remains a significant gap in addressing the high latency involved in establishing initial beams using narrow beams.

To tackle this problem, we propose a sensing-assisted BF method aimed at significantly reducing the latency of initial beam establishment. The core idea of the proposed method involves identifying the materials of the reflectors in the environment and estimating the Reflection Losses (RLs) for each beam direction based on the material infor-mation. The BS first scans the beam directions associated with reflectors that exhibit low RL. This strategy greatly increases the likelihood of quickly finding a trajectory with a low total Path Loss (PL), thereby expediting the initial beam alignment process.

The organization of this paper is as follows: Section 2 reviews the material sensing techniques employed in JCAS networks. Section 3 introduces a novel initial beam establishment method that uses material sensing. In Section 4, we present the simulation results for two scenarios and offer insights drawn from our research. Finally, Section 5 draws the conclusions.

Table 1 – Permittivity and conductivity values measured by ITU and Hexa-X for nine indoor and outdoor common building materials

Material	ε_r	σ_c	σ_d
Glass	6.31	0.0036	1.3394
Plaster	2.73	0.0085	0.9395
Plywood	1.8	0.006	1
Glass wool	1.2	0.002	1.2
Polystyrene	1.05	0.000008	1.1
Marble	7.074	0.0055	0.9262
Concrete	5.24	0.0462	0.7822
brick	3.91	0.0238	0.16
metal	1	10^7	0

2. RL-BASED MATERIAL IDENTIFICATION AND SUPPORTING TECHNOLOGIES

2.1 Overview of RL-based material identification

Our previous work [13, 14, 15] has developed a series of RL-based methods for material identification within JCAS systems. The fundamental principle of these methods is that RL is influenced by the electrical properties of materials, such as permittivity, conductivity, incident angle, as well as surface roughness. The Fresnel reflection coefficient r_{TE} for Transverse Electric (TE) polarization is given by

$$r_{TE}(\theta_i) = \frac{\cos\theta_i - \sqrt{\eta - \sin^2\theta_i}}{\cos\theta_i + \sqrt{\eta - \sin^2\theta_i}} \qquad (1)$$

where θ_i is the incident angle, η is the relative permittivity of a specific material, and

$$\eta = \varepsilon_r - j\frac{17.98\sigma_c f_c^{\sigma_d}}{f_c} \qquad (2)$$

and f_c represents the carrier frequency, ε_r is the dielectric relative permittivity, σ_c and σ_d are the material properties that determine the dielectric relative conductivity. The values for ε_r, σ_c, and σ_d for nine common indoor and outdoor building materials have been documented by ITU [16] and Hexa-X [17], and are tabulated in Table 1. The RL for TE polarization can be calculated by [17]

$$RL(\theta_i) = 10\log_{10}|\frac{1}{r_{TE}(\theta_i)}|^2 \qquad (3)$$

Additionally, RL values can be obtained through direct measurements [14]. The total PL for a trajectory in decibels is calculated as the difference between the transmitted power P_{TX} at the Transmitter (TX) side and the received power P_{RX} at the receiver (RX) side:

$$PL = P_{TX} - P_{RX} \qquad (4)$$

The total PL for a single-bounce reflection trajectory with length d can be expressed as the sum of Free Space Path Loss (FSPL) and RL:

$$PL(f_c, d, \theta_i) = FSPL(f_c, d) + RL(\theta_i) \qquad (5)$$

FSPL can be calculated by Friis' equation:

$$FSPL(f_c, d) = 20\log_{10}(d) + 20\log_{10}(f_c) + 20\log_{10}(\frac{4\pi}{c}) \quad (6)$$

where c is light speed.

By using the measured P_{RX} along with trajectory information, including length d and incident angle θ_i, we can determine the RL for a single-bounce reflection trajectory. Various building materials exhibit distinct RLs even at the same incident angle [15]. Based on this fact, the material of a reflecting surface can be inferred by matching the RL for a specific incident angle in an RL database.

2.2 Supporting technologies for RL-based material identification

The effective operation of RL-based material identification systems relies on several critical supporting technologies.

First, the frequency of radio waves significantly impacts the reliability of RL measurements. Equation *(1)* for calculating $r_{TE}(\theta_i)$ assumes that radio waves do not penetrate the material layer. If penetration occurs, it affects the RL measurement. In such cases, the Fresnel reflection coefficient $r_{TE, slab}$ for a slab is adjusted as follows [15]:

$$r_{TE, slab}(\theta_i) = \frac{r_{TE}(\theta_i)(1 - \exp(-j2q))}{1 - r_{TE}^2(\theta_i)\exp(-j2q)} \qquad (7)$$

where

$$q = 2\pi h f_c \sqrt{\eta - \sin^2\theta_i} \qquad (8)$$

and h is the thickness of the slab.

From equation *(7)*, it is evident that the assumption of non-penetration holds true when building materials are sufficiently thick or using high frequency radio waves (e.g., 100 GHz and above) to ensure stable reflection, and therefore, reliable RL measurements [15].

Additionally, the Fresnel equation *(1)* is valid for smooth surfaces. Most indoor surfaces can typically be considered smooth for RL estimation. However, for outdoor surfaces, the scattering loss induced by surface roughness must be considered. In these scenarios, the Fresnel reflection coefficient r_{TE} should be adjusted by the Rayleigh roughness factor ρ [18]:

$$r_{TE, roughness}(\theta_i) = \rho r_{TE}(\theta_i) \qquad (9)$$

where $r_{TE, roughness}(\theta_i)$ incorporates surface roughness effects. The Rayleigh roughness factor ρ is defined as [18]:

$$\rho = \exp(-\frac{8\pi^2\sigma_R^2 f_c^2\cos^2\theta_i}{c^2}) \qquad (10)$$

with σ_R as the standard deviation of surface roughness.

Waveguide theory is crucial for RL measurements in specific building structures like corridors and tunnels, which act as waveguides. Radio wave propagation within a waveguide is subject to attenuation over distance, impacting RL measurement accuracy. Understanding waveguide effects is essential for precise material identification in environments with such structures.

Interference mitigation is another critical aspect for reliable RL-based material identification. Two primary sources of interference must be addressed. Within a single BS, simultaneous transmission of multiple beams can lead to sidelobe interference with the main beam used for RL measurement, thereby reducing RL measurement accuracy. Effective sidelobe cancellation techniques are essential to minimize this interference. In multiple BS scenarios, interference from neighboring BSs' downlink communication or sensing signals can also disrupt RL measurements. This inter-cell interference is particularly challenging in dense urban environments with closely spaced BSs. Advanced interference mitigation strategies are essential to reduce the impact of neighboring BS signals.

By integrating these supporting technologies, the RL-based system can achieve higher efficiency and reliability in material identification.

3. MATERIAL SENSING-BASED INITIAL BEAM ESTABLISHMENT METHOD

In 5G NR, the BS conducts an exhaustive sweep of all beam directions using a predefined scanning pattern, such as a sawtooth pattern, to detect communication devices located at unknown positions. At higher frequency bands like mmWave and THz, this process becomes increasingly time-consuming due to the necessity of scanning a vast number of beam directions using narrow beams. Despite this complexity, the high directivity of narrow beams means that even reflecting trajectories can maintain robust connectivity. Therefore, the significant latency in establishing initial beams at these frequencies can be effectively mitigated by swiftly identifying a reflecting trajectory with low total PL.

As discussed in Section 2, the total PL of a reflecting trajectory is comprised of FSPL and RL. When a BS conducts a search for UE by sweeping a narrow beam in a specific direction, it is uncertain whether a viable path
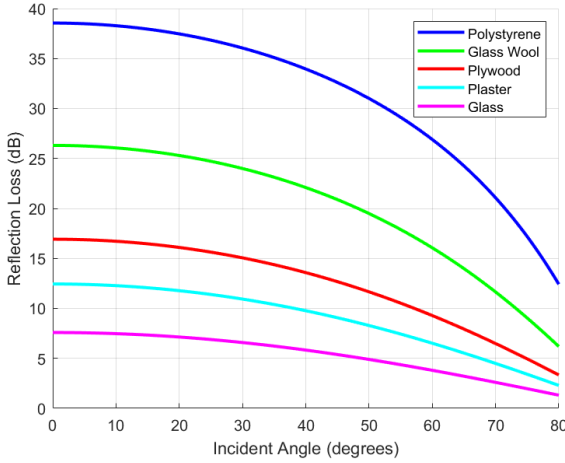
Figure 1 – RLs induced by five common indoor building materials at 100 GHz

exists between them. Even if such a path exists, the length of the path, which contributes to FSPL, cannot be predicted prior to establishing a connection. However, RL can be anticipated if material information of the environment is known in advance. Figure 1 illustrates the RLs induced by surfaces made of five common indoor building materials, namely glass, plaster, plywood, glass wool, and polystyrene, at incident angles ranging from 0° to 80°. From Figure 1, we can see that glass surfaces induce significantly lower RLs compared to other materials. Consequently, beam directions targeting glass surfaces are more likely to find and establish a reflecting trajectory with a lower total PL than those targeting other materials. Based on this analysis, we propose a material sensing-assisted beam sweeping method designed to reduce latency during the initial beam establishment. The method includes the following steps:

- Step 1: Import the three-Dimensional (3D) map of the environment and identify the material properties of objects using the methods outlined in [13, 14, 15].
- Step 2: Prioritize beam directions based on the materials of reflectors within the environment. Beam directions targeting materials with lower RL are given higher priority for beam sweeping, and vice versa. This prioritization determines the order of beam sweeping.
- Step 3: During the initial beam establishment phase, the BS scans the beam directions in order of decreasing priority and transmits SSBs. The UE measures and reports the RSRP of these SSBs. If the RSRP exceeds a predefined threshold, the connection is established immediately, foregoing further sweeping of the rest of the beam directions.
- Step 4 (optional): Since the trajectory established in step 3 may not be optimal, a beam update process can be initiated to search for the best trajectory, such as a Line-Of-Sight (LOS) trajectory.

The material sensing-assisted initial beam establishment method is summarized in Algorithm 1.

Algorithm 1 Material Sensing-Assisted Initial Beam Establishment

---

Require: 3D map of the environment, material properties of objects, predefined threshold for RSRP
Ensure: Established beam direction
1: Import the 3D map of the environment and identify the material properties of objects.
2: **for** each material **do**
3:   Calculate RL using the Fresnel reflection coefficient:
4:   $r_{\text{TE}}(\theta_{\text{i}}) = \frac{\cos\theta_{\text{i}} - \sqrt{\eta - \sin^2\theta_{\text{i}}}}{\cos\theta_{\text{i}} + \sqrt{\eta - \sin^2\theta_{\text{i}}}}$
5:   $\eta = \varepsilon_r - \text{j}\frac{17.98\sigma_c f_{\text{c}}^{\sigma_d}}{f_{\text{c}}}$
6:   $\rho = \exp(-\frac{8\pi^2\sigma_{\text{R}}^2 f_{\text{c}}^2 \cos^2\theta_{\text{i}}}{c^2})$
7:   $RL(\theta_{\text{i}}) = 10\log_{10}|\frac{1}{\rho r_{\text{TE}}(\theta_{\text{i}})}|^2$
8: **end for**
9: Prioritize beam directions based on the materials of reflectors within the environment.
10: **for** each beam direction in decreasing priority **do**
11:   Transmit SSBs.
12:   Measure and report the RSRP.
13:   **if** RSRP exceeds the predefined threshold **then**
14:     Establish the connection.
15:     **break**
16:   **end if**
17: **end for**
18: **if** Optional: Perform beam update process **then**
19:   Search for the optimal trajectory.
20: **end if**

---

4. SIMULATION RESULTS

To validate the effectiveness of the proposed method, we present MATLAB simulation results for both an indoor office scenario and an outdoor dense urban scenario in this section.

4.1 Indoor simulation results

As depicted in Figure 2, a 3D map of an office with dimensions of 5 m×8 m×3.2 m is imported in standard tessellation language format, which is a widely used 3D map format that can be generated by various 3D modeling software [19]. The office features different materials, which are represented by different colors for each surface: polystyrene (green) for the front wall, glass (blue) for the back wall, glass wool (red) for the side walls, plywood (yellow) for the floor, tables, chairs, and the partition wall, and plaster (gray) for the ceiling. Four BSs (BS1-BS4) are positioned near the four upper corners of the office. To simplify the simulation, the UE is restricted to twenty-eight predetermined positions (P1-P28). Ray tracing is used to analyze the single-bounce reflection
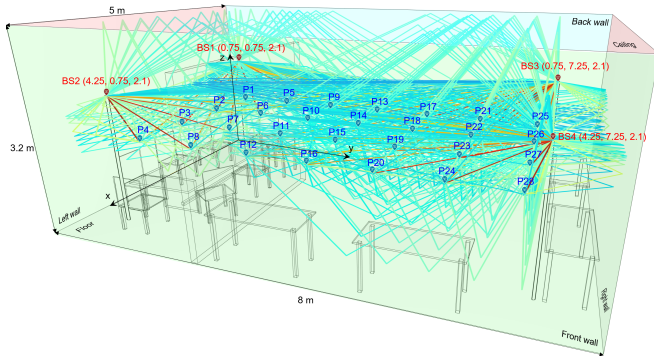
Figure 2 – An illustration of a simulated office featuring 4 BSs and 28 UE positions (P1-P28), and the trajectories calculated by ray tracing between all BS-UE position pairs.
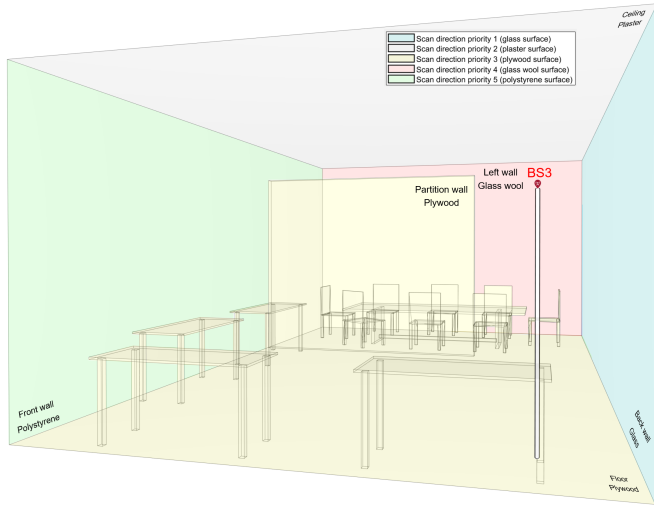
Figure 3 – Perspective view of the office as seen behind BS3

trajectories between each BS-UE position pair, which are shown in Figure 2, totaling 430.

BS3 at (0.75, 7.25, 2.1) and a UE at P14 (2, 4, 1.3) are selected as an example to demonstrate how the proposed method can decrease the latency of initial beam establishment. Figure 3 shows the office's perspective from a viewpoint behind BS3. According to Figure 1, the back wall made of glass exhibits the lowest RL, prompting BS3 to prioritize scanning towards these beam directions first (scan direction priority 1). If no viable trajectory is identified, the scanning sequence progresses to the ceiling (scan direction priority 2), and so forth. The antenna configuration used in the simulation includes a FOV of ±70° in both azimuth and elevation, with a half-power beamwidth of 5°. Figure 4 displays the five single-bounce reflection trajectories between BS3 and the UE at P14 as determined by ray tracing. Details of these trajectories, including the materials of reflectors, path lengths, FSPL, incident angles, RL, and total PL, are listed in Table 2. As seen from Table 2, trajectory 1 has a significantly lower RL compared to others. Despite not having the lowest FSPL, trajectory 1 achieves the lowest total PL, making it the most favorable option for establishing a non-LOS trajectory between BS3 and the UE at P14.
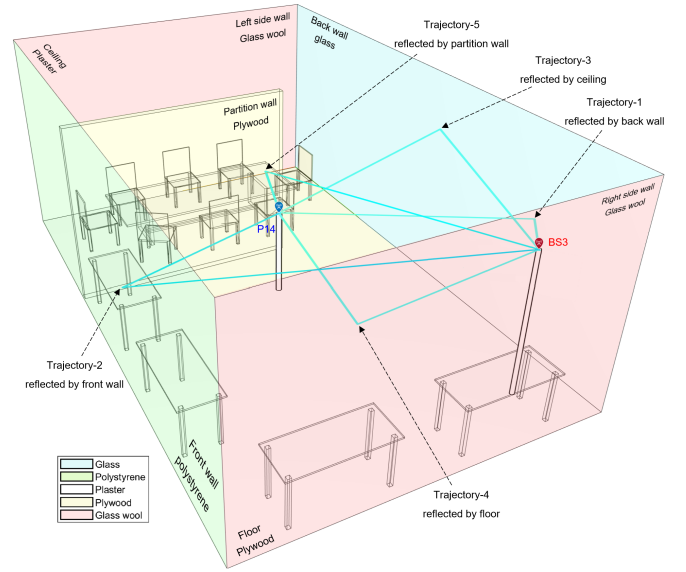

Figure 4 – Five single-bounce reflection trajectories between BS3 and the UE at P14 in the indoor office scenario

Figure 5 illustrates what BS3 can "see" within its FOV in the office. The cyan, green, black, yellow, and orange markers "○" indicate the Directions of Departure (DoD) for trajectories 1 to 5 shown in Figure 4. For example, a beam targeted at the cyan marker will reflect off the back wall and be received by the UE at P14, thus establishing trajectory 1 between BS3 and the UE at P14. The dashed circles represent potential beam positions that BS3 can aim at, totaling 784 beam directions. This indicates that an exhaustive beam search would traditionally require scanning all 784 directions before establishing a connection. However, with the proposed method, BS3 initially scans the glass back wall, assumed to scan in a sawtooth pattern: sweeping the beam horizontally from left to right at the bottom, then moving up in elevation as indicated by the blue polygonal arrow in Figure 5. After just 34 sweeps, trajectory 1 is established, eliminating the need to scan the remaining 750 beam directions. This results in a reduction of initial beam establishment latency by 95.7% (750/784), a significant improvement over the exhaustive beam search method.

To evaluate whether the proposed method consistently perform well across different scenarios, we applied it to all BS-UE position pairs and analyzed the results. Figure 6 presents the total PLs for all the trajectories depicted in Figure 2. The x-axis lists all the BS-UE position pairs from BS1-P1 to BS4-P28, while the y-axis shows the total PLs of these trajectories. The total PLs of trajectories reflected by glass, plaster, plywood, glass wool, and polystyrene are indicated by blue, white, yellow, red, and green dots, respectively. Figure 6 reveals that the trajectories reflected by glass surfaces are most likely the best, with 73.8% of the pairs (62 out of 84 pairs) achieving the best results when reflecting off glass, and the remaining 26.2% (22 pairs) having optimal reflections off plaster surfaces. This indicates a 73.8% success rate in identifying the

Table 2 – Trajectory information between BS3 and UE at P14 in an indoor scenario in Figure 4, and between BS5 and UE at P29 in an outdoor scenario in Figure 10

Scenario	Trajectory	Reflector	Material	Path length (m)	FSPL (dB)	$\theta_i(°)$	RL (dB)	PL (dB)
Indoor office	1	Back wall	Glass	4.6	85.71	50.7	7.08	92.79
	2	Front wall	Polystyrene	8	90.51	24.9	38.31	128.82
	3	Ceiling	Plaster	4.43	85.16	49.3	11.14	96.3
	4	Floor	Plywood	4.87	86.2	45.6	15.36	101.56
	5	Partition wall	Plywood	5.97	87.97	14.3	16.9	104.87
Outdoor dense urban	6	Building 1	Concrete	460.63	125.72	13.3	34.14	159.86
	7	Building 1	Metal	459.64	125.7	12.5	1.64	127.34
	8	Building 2	Brick	236.47	119.92	25.1	44.79	164.71
	9	Building 3	Marble	170.74	117.08	41.8	10.57	127.65
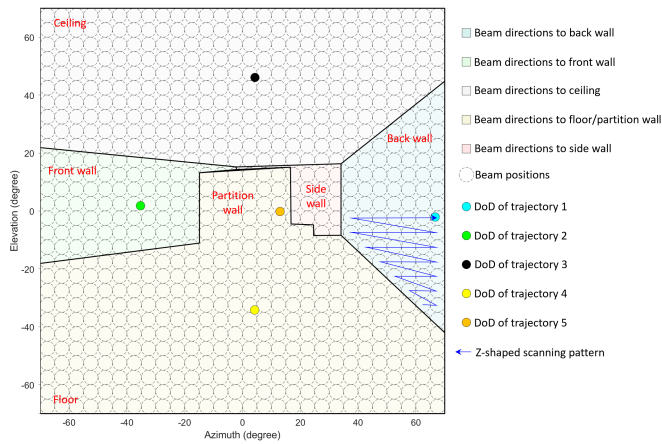
Figure 5 – The view from BS3 showing the DoD for trajectories 1-5 between BS3 and the UE at P14

best trajectory by initially scanning the glass surfaces. The reason for the unsuccessful cases where trajectories reflected by glass are not the best trajectories is due to their significantly longer path lengths compared to those reflected by plaster. Although glass has a lower RL, the longer path length results in a higher FSPL, therefore, a higher total PL. However, such cases are relatively rare.

To evaluate the latency performance of the proposed method, we analyzed the establishment latencies for all trajectories reflected by the glass back wall. Figures 7(a)-(d) provide views from BS1 to BS4, with cyan markers indicating the DoD of trajectories reflected by the glass back wall. Employing the sawtooth scanning pattern, the average number of beam sweeps required to identify these trajectories is 36.4. This reveals that the average latency for initial beam establishment using the proposed method is reduced by 95.4% compared to a traditional exhaustive beam search. Furthermore, all reflection points are centrally located on the back wall, as illustrated in Figures 7(a)-(d). This is because the simulation restricts the height of the UEs to 1.3 m, a realistic height for portable communication devices. This height constraint enhances the likelihood of reflections occurring at central parts on the walls. This observation suggests that tar-

geting the center of the back wall initially could further reduce the latency. Therefore, the use of the distribution of communication devices and designing new scanning patterns could serve as effective strategies to decrease latency even more.

4.2 Outdoor simulation results

To evaluate the effectiveness of the proposed method in outdoor environments, we extended our simulation to a dense urban scenario. As illustrated in Figure 8, we imported the map of Chicago from OpenStreetMap [20]. We defined a region with several city blocks and extracted the 3D building data. Each building surface was randomly assigned one of five common outdoor materials, with specific colors: metal (black), glass (cyan), marble (purple), concrete (gray), and brick (red). The RLs induced by these materials at incident angles from 0° to 80° are shown in Figure 9. It is worth noting that the roughness of concrete and brick surfaces in outdoor scenarios cannot be omitted, σ_R of concrete and brick surfaces are set to 2.5 mm.

We randomly placed ten BS-UE pairs within the city blocks. Using ray tracing, we adjusted the BS-UE positions until each pair had at least two single-bounce reflection trajectories. This process was repeated ten times to gather diverse trajectory data from 100 BS-UE pairs, allowing us to assess the proposed method under varying conditions. Figures 8(a) and 8(b) illustrate the results from two of these ten simulations.

In the example scenario depicted in Figure 10, which shows a section of the city blocks, we analyzed one of the 100 BS-UE pairs to illustrate the effectiveness of the proposed method for outdoor scenarios. According to the proposed method, BS5 should prioritize scanning the metal surface of Building 1 first due to its lower RL. As shown in Table 2, the single-bounce reflection trajectory involving the metal surface (trajectory 7) exhibited
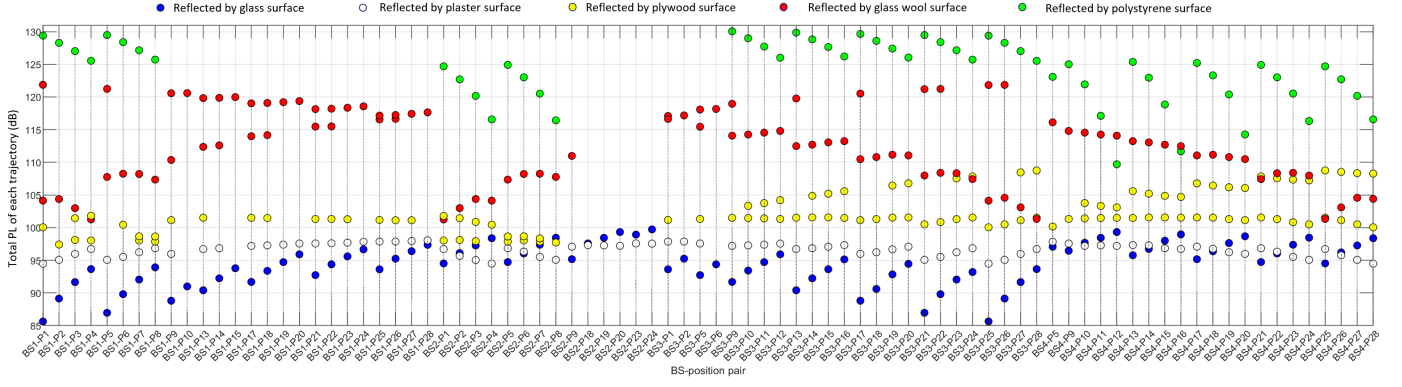
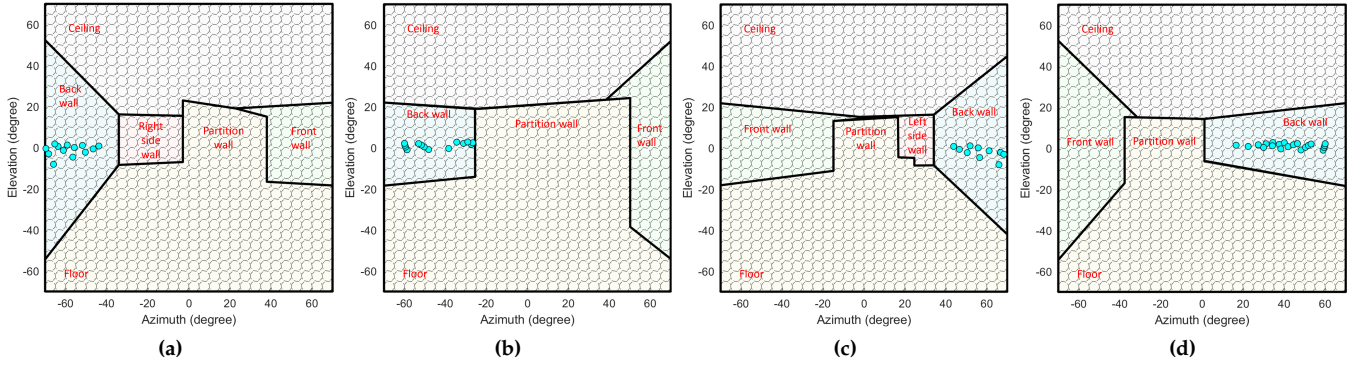**Figure 6** – Total PLs for the 430 trajectories in Figure 2

Figure 7 – Views and DoD of trajectories reflected by the back wall as seen from (a) BS1 (b) BS2 (c) BS3 (d) BS4
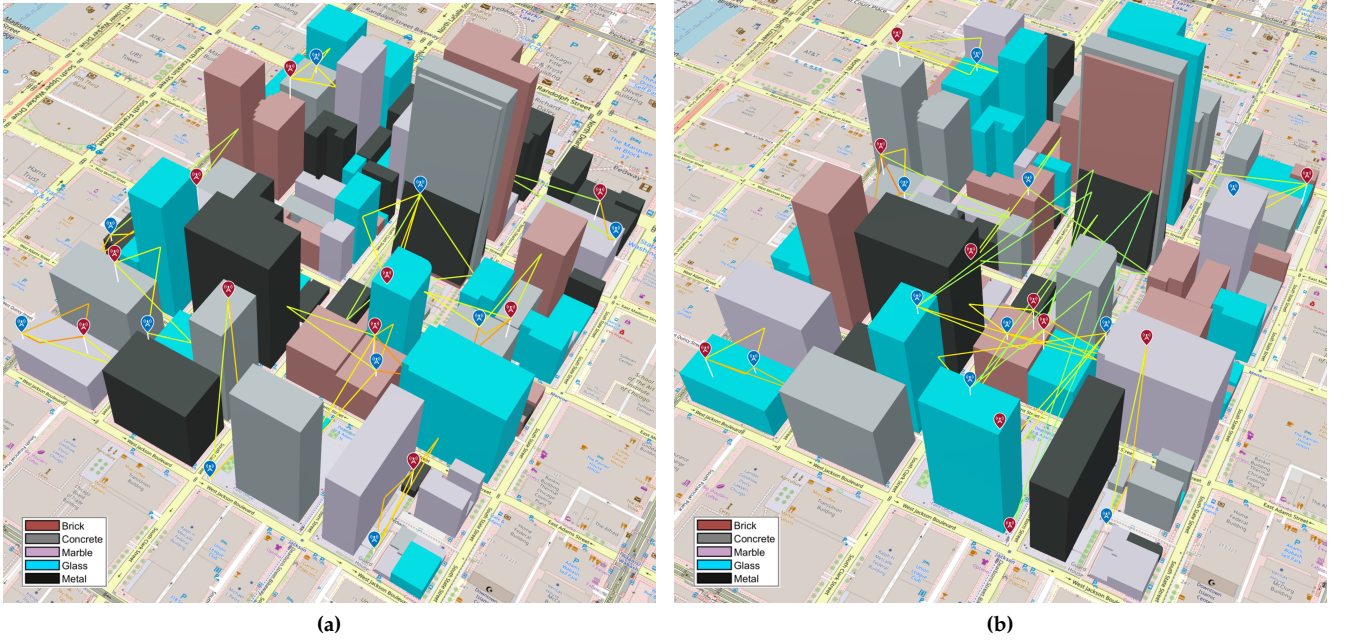

Figure 8 – Views of city blocks in an outdoor dense urban scenario. The building materials are randomly assigned, and ten BS-UE pairs with their single-bounce reflection paths are randomly placed within the blocks. (a) and (b) show the results from two different simulations
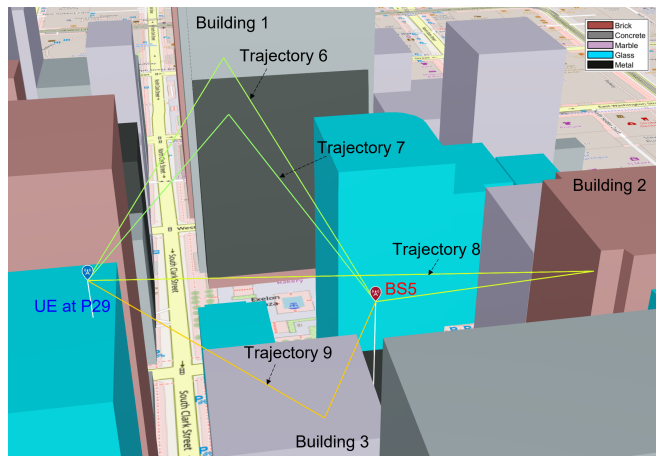
the lowest total PL. This outcome is attributed to the significantly lower RL of metal surfaces compared to other materials. Despite the relatively long path length of 459.64 m, the total PL of trajectory 7 was the lowest, making it the most favorable path for beam establishment.
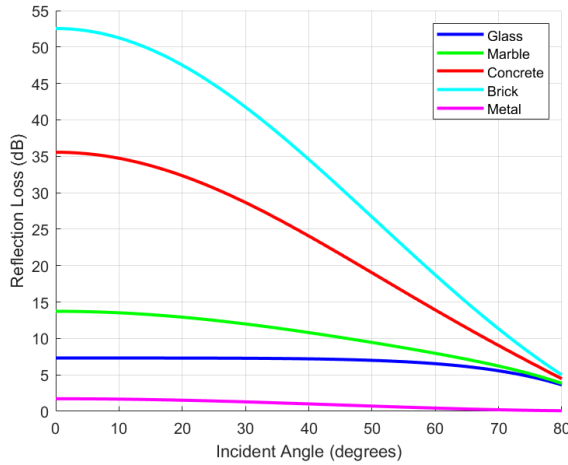
Figure 9 – RLs induced by five common outdoor building materials at 100 GHz

Figure 10 – Four single-bounce reflection trajectories between BS5 and the UE at P29 in the outdoor dense urban scenario

The simulation results for all 100 BS-UE pairs demonstrate the effectiveness of the proposed method. The method successfully established the optimal path by prioritizing the scanning of surfaces with low RL in 66% of the cases. This high success rate validates the method's capability to significantly reduce the initial beam establishment latency by leveraging material sensing.

4.3 Discussions

The proposed method's effectiveness can be further enhanced by integrating it with existing technologies such as hierarchical beam search algorithms and DNN-based beam search algorithms. For example, as depicted in Figure 5, the narrow beams directed towards the back wall can be consolidated into broader beams. This modification allows the hierarchical beam search algorithms to be combined effectively with the proposed method. Additionally, DNN-based beam search algorithms can be utilized to decrease latency further by specifically measuring the RSRP from a subset of all narrow beams aimed at the back wall.

The proposed method demonstrated a higher success rate in indoor scenarios compared to outdoor scenarios. This discrepancy can be attributed to several factors. In the indoor office scenario presented in this paper, there is always a low RL path via glass reflection between the BS and UE. However, in the outdoor dense urban scenario, the randomly placed BS and UE pairs do not always have a single-bounce reflection trajectory with low RL, such as those involving metal or glass surfaces.

Another factor is the significant variation in path lengths for single-bounce reflections in outdoor environments. The outdoor paths can vary greatly in length, and since FSPL increases by approximately 6 dB for every doubling of the path length, this can overshadow the influence of RL on the total PL. In contrast, in indoor scenarios, the path lengths for different single-bounce reflection trajectories between the BS and UE are generally more consistent, reducing the impact of path length variations on the total PL.

Moreover, the outdoor environment introduces more complexity and variability due to factors like building geometry, surface roughness, and environmental obstacles, which can further affect the reflection characteristics and the accuracy of RL estimation.

Future work could explore the integration of more sophisticated environmental modeling techniques and adaptive algorithms that dynamically adjust to the specific characteristics of the deployment scenario. Additionally, incorporating machine learning models to predict the most likely successful beam directions based on historical data and real-time sensing information could further improve the robustness and efficiency of the proposed method in diverse environments.

5. CONCLUSION

Sensing-assisted communications represent a promising technique within JCAS systems. In this paper, we introduced a material sensing-assisted BF method designed to significantly reduce the latency of initial beam establishment in high frequency bands. By estimating RL based on pre-identified material information in the environment, and prioritizing beam directions with lower RL, the BS can efficiently establish a suitable beam pair without the need to scan all possible directions. This approach markedly decreases the time required to establish initial beams. The simulation results demonstrated the effectiveness of the proposed method in both indoor and outdoor environments. The proposed method achieved a 73.8% success rate in establishing the optimal single-bounce reflection path in the indoor office scenario and

a 66% success rate in the outdoor dense urban scenario. This material sensing-assisted BF method is poised to enable 6G networks to meet the demanding low latency requirements essential for ultra-reliable low-latency communications use cases.

ACKNOWLEDGEMENT

REFERENCES

[1] Harri Holma, Harish Viswanathan, and Preben Mogensen. *Extreme massive MIMO for macro cell capacity boost in 5G-Advanced and 6G*. White paper. Nokia Bell Labs, 2021.

[2] Theodore S. Rappaport, Yunchou Xing, Ojas Kanhere, Shihao Ju, Arjuna Madanayake, Soumyajit Mandal, Ahmed Alkhateeb, and Georgios C. Trichopoulos. "Wireless Communications and Applications Above 100 GHz: Opportunities and Challenges for 6G and Beyond". In: *IEEE Access* 7 (2019), pp. 78729–78757. DOI: 10.1109/ACCESS.2019.2921522.

[3] Song Noh, Jiho Song, and Youngchul Sung. "Fast Beam Search and Refinement for Millimeter-Wave Massive MIMO Based on Two-Level Phased Arrays". In: *IEEE Transactions on Wireless Communications* 19.10 (2020), pp. 6737–6751. DOI: 10.1109/TWC.2020.3004916.

[4] Aleksandar Ichkov, Simon Häger, Petri Mähönen, and Ljiljana Simić. "Comparative Evaluation of Millimeter-Wave Beamsteering Algorithms Using Outdoor Phased Antenna Array Measurements". In: *2022 19th Annual IEEE International Conference on Sensing, Communication, and Networking (SECON)*. 2022, pp. 497–505. DOI: 10.1109/SECON55815.2022.9918162.

[5] B. Kim, Y. Sagduyu, T. Erpek, and S. Ulukus. "Adversarial Attacks on Deep Learning Based mmWave Beam Prediction in 5G And Beyond". In: *2021 IEEE Statistical Signal Processing Workshop (SSP)*. 2021, pp. 590–594. DOI: 10.1109/SSP49050.2021.9513738.

[6] Tarun S. Cousik, Vijay K. Shah, Jeffrey H. Reed, Tugba Erpek, and Yalin E. Sagduyu. "Fast Initial Access with Deep Learning for Beam Prediction in 5G mmWave Networks". In: *MILCOM 2021 - 2021 IEEE Military Communications Conference (MILCOM)*. 2021, pp. 664–669. DOI: 10.1109/MILCOM52596.2021.9653011.

[7] Yuqiang Heng, Jianhua Mo, and Jeffrey G. Andrews. "Learning Site-Specific Probing Beams for Fast mmWave Beam Alignment". In: *IEEE Transactions on Wireless Communications* 21.8 (2022), pp. 5785–5800. DOI: 10.1109/TWC.2022.3143121.

[8] J. Andrew Zhang, Fan Liu, Christos Masouros, Robert W. Heath, Zhiyong Feng, Le Zheng, and Athina Petropulu. "An Overview of Signal Processing Techniques for Joint Communication and Radar Sensing". In: *IEEE Journal of Selected Topics in Signal Processing* 15.6 (2021), pp. 1295–1315. DOI: 10.1109/JSTSP.2021.3113120.

[9] Fan Liu, Weijie Yuan, Christos Masouros, and Jinhong Yuan. "Radar-Assisted Predictive Beamforming for Vehicular Links: Communication Served by Sensing". In: *IEEE Transactions on Wireless Communications* 19.11 (2020), pp. 7704–7719. DOI: 10.1109/TWC.2020.3015735.

[10] Weijie Yuan, Fan Liu, Christos Masouros, Jinhong Yuan, Derrick Wing Kwan Ng, and Nuria González-Prelcic. "Bayesian Predictive Beamforming for Vehicular Networks: A Low-Overhead Joint Radar-Communication Approach". In: *IEEE Transactions on Wireless Communications* 20.3 (2021), pp. 1442–1456. DOI: 10.1109/TWC.2020.3033776.

[11] Xiao Meng, Fan Liu, Christos Masouros, Weijie Yuan, Qixun Zhang, and Zhiyong Feng. "Vehicular Connectivity on Complex Trajectories: Roadway-Geometry Aware ISAC Beam-Tracking". In: *IEEE Transactions on Wireless Communications* 22.11 (2023), pp. 7408–7423. DOI: 10.1109/TWC.2023.3250442.

[12] Zhen Du, Fan Liu, Weijie Yuan, Christos Masouros, Zenghui Zhang, Shuqiang Xia, and Giuseppe Caire. "Integrated Sensing and Communications for V2I Networks: Dynamic Predictive Beamforming for Extended Vehicle Targets". In: *IEEE Transactions on Wireless Communications* 22.6 (2023), pp. 3612–3627. DOI: 10.1109/TWC.2022.3219890.

[13] Yi Geng, Vijaya Yajnanarayana, Ali Behravan, Erik Dahlman, and Deep Shrestha. "Study of Reflection-Lass-Based Material Identification from Common Building Surfaces". In: *2021 Joint European Conference on Networks and Communications & 6G Summit (EuCNC/6G Summit)*. 2021, pp. 526–531. DOI: 10.1109/EuCNC/6GSummit51104.2021.9482524.

[14] Yi Geng, Deep Shrestha, Vijaya Yajnanarayana, Erik Dahlman, and Ali Behravan. "Joint scatterer localization and material identification using radio access technology". In: *EURASIP Journal on Wireless Communications and Networking* 2022.87 (2022). DOI: 10.1186/s13638-022-02167-7.

[15] Yi Geng. "Map-Assisted Material Identification at 100 GHz and Above Using Radio Access Technology". In: *2022 Joint European Conference on Networks and Communications & 6G Summit (EuCNC/6G Summit)*. 2022, pp. 476–481. DOI: 10.1109/EuCNC/6GSummit54941.2022.9815822.

[16] Recommendation ITU-R P.2040-2 (2021). *Effects of building materials and structures on radiowave propagation above about 100 MHz*. Tech. rep. International Telecommunication Union.

[17] Ahmad Nimr, Matti Leinonen, and Melisa Sarajlic. *Deliverable D2.3 radio models and enabling techniques towards ultra-high data rate links and capacity in 6G*. Deliverable D2.3. Hexa-X, 2023.

[18] Petr Beckmann and André Spizzichino. *The Scattering of Electromagnetic Waves from Rough Surfaces*. Norwood, MA: Artech House, 1987.

[19] Gabriel Avelino Sampedro, Syifa Maliah Rachmawati, Khurboev Shakhzodbek Dilshodbek Ugli, Dong-Seong Kim, and Jae-Min Lee. "SimuPrint: A Printing Path Simulation Tool for Additive Manufacture". In: *2022 13th International Conference on Information and Communication Technology Convergence (ICTC)*. 2022, pp. 906–909. DOI: 10.1109/ICTC55196.2022.9952755.

[20] OpenStreetMap contributors. *OpenStreetMap*. https://www.openstreetmap.org. Licensed under the Open Data Commons Open Database License (ODbL), https://opendatacommons.org/licenses/odbl/. 2024.

AUTHOR

YI GENG received his B.S. degree from Shandong University in Jinan, China, in 2000, and his M.S. degree from Nanjing University of Posts and Telecommunications in Nanjing, China, in 2007. Since then, he has been actively engaged in the research, development, and customer support of mobile networks from 2G to 6G. Currently, he serves as a researcher in the field of 6G Joint Communications And Sensing (JCAS) at CICT Mobile, China. His research interests focus on JCAS and aerial communications.